Mechanics reveals the biological trigger in wrinkly fingers

P. Sáez [a,*], A. M. Zöllner[b]

[a] *Laboratori de Calcul Numeric (LaCaN), Universitat Politecnica de Catalunya, Barcelona, Spain.* [b] *Department of Mechanical Engineering, Stanford University, Stanford, CA 94305, US*

* pablo.saez@upc.edu

Abstract

Fingertips wrinkle due to long exposure to water. The biological reason for this morphological change is unclear and still not fully understood. There are two main hypotheses for the underlying mechanism of fingertip wrinkling: the 'shrink' model (in which the wrinkling is driven by the contraction of the lower layers of skin, associated with the shrinking of the underlying vasculature), and the 'swell' model (in which the wrinkling is driven by the swelling of the upper layers of the skin, associated with osmosis). In reality, contraction of the lower layers of the skin and swelling of the upper layers will happen simultaneously. However, the relative importance of these two mechanisms to drive fingertip wrinkling also remains unclear. Simulating the swelling in the upper layers of skin alone, which is associated with neurological disorders, we found that wrinkles appeared

above an increase of volume of $\approx 10\%$. Therefore, the upper layers can not exceed this swelling level in order to not contradict *in vivo* observations in patients with such neurological disorders. Simulating the contraction of the lower layers of the skin alone, we found that the volume have to decrease a $\approx 20\%$ to observe wrinkles. Furthermore, we found that the combined effect of both mechanisms leads to pronounced wrinkles even at low levels of swelling and contraction when individually they do not. This latter results indicates that the collaborative effect of both hypothesis are needed to induce wrinkles in the fingertips. Our results demonstrate how models from continuum mechanics can be successfully applied to testing hypotheses for the mechanisms that underly fingertip wrinkling, and how these effects can be quantified.

Keywords: Biomechanics, wrinkly fingers, finite element method, continuum mechanics

1 Motivation

Almost all of us have experienced wrinkly fingers after a long bath, mainly in the feet and hands and particularly on the tip of the toes (see Fig 1). For a long time wrinkly fingers were attributed to osmosis[7], which leads to the swelling of the epidermis as water gets into the tissue. However, this hypotheses was challenged when researchers noted that diseases of the sympathetic function cancel the wrinkling process[47,7,55]. Nerves under the skin trigger vasoconstriction mechanisms that reduce the volume of the tissue under the epidermis[56]. Apart from these underlying mechanisms, the wrinkling process was also

described by evolutionary purposes[23,33]. The formation of wrinkles has been demonstrated to give a better grip on objects when our hands are wet or underwater[33]. The hypotheses of rain-tread-type or tire shape of the wrinkles also supports the biological function of better grip, creating channels that allow water to flow away from the finger as we grab an object[10].

The skin, the biological system that concerns this problem, is made of three main layers: epidermis, dermis and the hypodermis [37]. The epidermis is the most external layer consisting of dead corneocyte cells in the stratum corneum and different living cells in the basal layers. The stratum corneum is the most external and stiffest layer in the epidermis. The keratin content forms an open mesh and allows the absorption of water which makes the epidermis swell. This layer is a natural barrier from the environment. In the inner layer, the dermis is made of 2 sublayers, the papillary and reticular stratum. The main components of the dermis are fibroblast, macrophages and extracellular components such as elastin and collagen. The papillary sublayer contains the terminal blood capillaries and Meissner Corpuscles. We can also find the so-called glomus bodies, which are linked to the sympathetic nervous system. They are responsible for sensing the external stimuli as temperature and humidity. The reticular layer is mainly composed of extracellular matrix components and provides strength and stiffness to the dermis. Under the dermis we find the subcutaneous tissue or hypodermis made of fibroblasts, adipose cells, macrophages and fat tissue.

In terms of the biomechanical description of the wrinkling process, the shrinking of the

hypodermis in combination with the swelling of the epidermis sets a classical mechanical problem of differentially swelling substrates[30,31,58,16]. Differential pattern formation has been studied due to differential swelling[32,59,51], as well as buckling phenomena in growing surfaces[3,25,44,14]. Numerical and theoretical approaches have been used to study the appearance of folds in the airwall[5,18,2], in arteries[39] or in idealized tube-like geometries[46,18,15]. Finite element approaches, together with bifurcation theory have also been used to investigate the folding pattern in the mammalian brain[8,9], wrinkles in the fingertips[17,53,13], fruits[41] and morphogenesis of the epithelium[12,13]. Flynn and co-workers studied the mechanics of wrinkles in the skin and its relation to ageing in a multilayer finite element model[21,22]. Probably, the work presented by Yin et al.[53] represents the closest approach to the model presented here. Yin and co-workers analyzed the effect of finger curvature, skin thickness and structure to understand the wrinkling phenomenon in the fingertips by computational and analytical means. However, they did not analyze the differential growth arising for the swelling and contraction of the different layers simultaneously. This is, from experimental observations, a key aspect in the formation of wrinkles.

Almost none of the previous works have dealt with the formation of water-induced wrinkles in the fingertip and among them, and as far as we know none analyze the coupling effect of the contraction and swelling mechanisms. In this work, we analyze the mechanisms that lead to wrinkly fingers by using well established computational models of volumetric changes, as referenced above. We use a computational mechanics framework to analyze the individual and coupled contributions of the contraction of the dermis and

Figure 1: Wrinkles on human fingertips (Photograph by Julia Haseleu / MDC, with permission). The figure showcases fingertip wrinkling after water immersion.

the swelling of the epidermis to underwater-induced fingertip wrinkling. Our results aim to solve this known but still open problem in biology and to conclude which one of these phenomena, and to what extend, is responsible for the wrinkly fingers in water immersion conditions.

2 Model of finger wrinkling

2.1 Continuum mechanics approach

Within the framework of finite growth (see reviews in the context of biological tissue[1,43,35,50]), the key kinematic assumption in our approach is the multiplicative decomposition of the deformation gradient $\mathbf{F}$ into an elastic part $\mathbf{F}_\mathrm{e}$ and a growth part $\mathbf{F}_\mathrm{g}$[49],

$$\mathbf{F} = \mathbf{F}_\mathrm{e} \cdot \mathbf{F}_\mathrm{g} \,. \tag{1}$$

We will parameterise the growth tensor exclusively in terms of a single scalar-valued variable, the growth multiplier ϑ[24,43,35]. Based on this definition, we can define the rest of the kinematic variables[42]. We denote the Jacobians of the elastic tensor and of the growth tensor as $J_\mathrm{e} = \det(\mathbf{F}_\mathrm{e})$ and $J_\mathrm{g} = \det(\mathbf{F}_\mathrm{g})$, respectively, such that $J = J_\mathrm{e}\, J_\mathrm{g}$. We can then introduce the elastic right Cauchy Green tensor $\mathbf{C}_\mathrm{e}$ in the following form.

$$\mathbf{C}_\mathrm{e} = \mathbf{F}_\mathrm{e}^\mathrm{t} \cdot \mathbf{F}_\mathrm{e} = \mathbf{F}_\mathrm{g}^{\text{-t}} \cdot \mathbf{C} \cdot \mathbf{F}_\mathrm{g}^{\text{-1}} \tag{2}$$

where $\mathbf{C}$ is the total right Cauchy Green tensor.

Next, we embed the kinematic characterization of growth into a hyperelastic baseline description[42,29]. To this end, we re-parametrize the Helmholtz strain energy function $\Psi(\mathbf{C}_\mathrm{e})$[34,35,50], which was initially parametrized in terms of the elastic deformation tensor $\mathbf{C}_\mathrm{e}$, in terms of the total deformation tensor $\mathbf{C}$ and the growth tensor $\mathbf{F}_\mathrm{g}$, such that $\Psi(\mathbf{C}, \mathbf{F}_\mathrm{g})$ and

$$\dot{\Psi} = \partial_{\mathbf{C}}\Psi : \dot{\mathbf{C}} + \partial_{\mathbf{F}_\mathrm{g}}\Psi : \dot{\mathbf{F}}_\mathrm{g} \tag{3}$$

Thermodynamic considerations motivate the introduction of the Piola-Kirchhoff stress,

$$\mathbf{S} = 2\partial_{\mathbf{C}}\Psi = 2\partial_{\mathbf{C}_\mathrm{e}}\Psi : \partial_{\mathbf{C}}\mathbf{C}_\mathrm{e} = \mathbf{F}_\mathrm{g}^{-1} \cdot \mathbf{S}_\mathrm{e} \cdot \mathbf{F}_\mathrm{g}^{-\mathrm{t}}\,, \tag{4}$$

with $\mathbf{S}_\mathrm{e} = \partial_{\mathbf{C}_\mathrm{e}}\Psi$. To derive the tangent moduli in the framework of open systems, essential for a consistent finite element implementation (see[34,24,50] for more details), we evaluate the total derivative of the $\mathbf{S}$ with respect to $\mathbf{C}$.

$$\begin{aligned} \mathbf{C} &= 2\mathrm{d}_{\mathbf{C}}\mathbf{S} = 2\partial_{\mathbf{C}}\mathbf{S}\big|_{\mathbf{F}_\mathrm{g}} + 2\partial_{\mathbf{C}}\mathbf{S}\big|_{\mathbf{F}} \\ &= 2\partial_{\mathbf{C}}\mathbf{S}\big|_{\mathbf{F}_\mathrm{g}} + 2\left[\partial_{\mathbf{F}_\mathrm{g}}\mathbf{S} : \partial_{\vartheta}\mathbf{F}_\mathrm{g}\right] \otimes \partial_{\mathbf{C}}\vartheta\big|_{\mathbf{F}} \end{aligned} \tag{5}$$

The first term of equation (5) represents the classical tangent moduli. We denote the elastic tangent modulus in the intermediate configuration by $\mathbf{C}_{\mathrm{e}} = 2\mathrm{d}_{\mathbf{C}_{\mathrm{e}}}\mathbf{S}_{\mathrm{e}}$, the same tensor in the initial, stress-free configuration by $\mathbf{C}$, and the elastic modulus in the current configuration by $\mathbf{c}_{\mathrm{e}}$, such that

$$\hat{\mathbf{C}}_{\mathrm{e}} = [\mathbf{F}_{\mathrm{g}}^{-1}\overline{\otimes}\mathbf{F}_{\mathrm{g}}^{-1}] : 2\mathrm{d}_{\mathbf{C}_{\mathrm{e}}}\mathbf{S}_{\mathrm{e}} : [\mathbf{F}_{\mathrm{g}}^{-\mathrm{t}}\overline{\otimes}\mathbf{F}_{\mathrm{g}}^{-\mathrm{t}}] \tag{6}$$

and

$$\mathbf{c} = [\mathbf{F}\overline{\otimes}\mathbf{F}] : \mathbf{C} : [\mathbf{F}^{\mathrm{t}}\overline{\otimes}\mathbf{F}^{\mathrm{t}}]\,. \tag{7}$$

with the abbreviated notations $\{\bullet\}\bar{\otimes}\{\circ\}_{ijkl} = \{\bullet\}_{ik}\{\bullet\}_{jl}$ and $\{\bullet\}\underline{\otimes}\{\circ\}_{ijkl} = \{\bullet\}_{il}\{\bullet\}_{jk}$.

Finally, we adopt a quasi-incompressible formulation of the elastic part of the strain energy function, frequently adopted for modeling of biological tissue (see e.g.[29]). Due to the high water content the deformation gradient $\mathbf{F}^e$ can be decoupled as $\mathbf{F}^e = \mathrm{J}^{e\,1/3}\bar{\mathbf{F}}^{\mathbf{e}}$ [20]. The isochoric part defines the volume-preserving part so $\bar{\mathbf{F}}^e$ is called the isochoric deformation gradient. Thereafter, we can define the additive decomposition of elastic part of the strain energy function as

$$\Psi = \Psi_{\mathrm{vol}}(J) + \Psi_{\mathrm{ich}}(\bar{\mathbf{C}}) \tag{8}$$

where Ψ_{vol} is associated with the volumetric part due to the high water content of the tissue. $\Psi_{\mathrm{ich}}(\bar{\mathbf{C}})$ is related to the isochoric contribution of the deformation gradients, therefore, the volume-preserving contribution. Following the Clausius-Plank inequality we are able to obtain the momentum fluxes by derivation of the Helmholtz free energy by its associated strain measure (see, e.g.,[42]) as described in Eq. 4 and 5.

2.2 Constitutive equations in the wrinkling process

To model the skin swelling and the hypodermic shrinking we will use the growth deformation gradient defined in Eq. 1. The contraction of the dermis, $\mathbf{F}_{\mathrm{g,\,dermis}}$, and the swelling of the epidermis, $\mathbf{F}_{\mathrm{g,\,epi}}$, are defined as

$$\mathbf{F}_{\mathrm{g,\,dermis}} = \mathbf{I}\,\vartheta_{\mathrm{dermis}} \tag{9}$$

and

$$\mathbf{F}_{\mathrm{g,\,epi}} = \mathbf{I} + [\,\vartheta_{\mathrm{epi}} - 1\,]\,[\,\mathbf{n}_x \otimes \mathbf{n}_x + \mathbf{n}_y \otimes \mathbf{n}_y\,] \tag{10}$$

respectively. $\mathbf{I}$ denotes the second order identity tensor, $\vartheta_{\mathrm{epi}} \in [1, \vartheta_{epi}^{max}]$ and $\vartheta_{\mathrm{dermis}} \in [\vartheta_{dermis}^{min}, 1]$ represent the variables controlling the increase and decrease of volume in the dermis and epidermis layers. ϑ_{epi}^{max} and ϑ_{dermis}^{min} is the maximum and minimum value achieved for the growth multiplier in the epidermis and dermis respectively. The contraction in the hypodermic tissue is assumed to be isotropic while the swelling, the swelling of the epidermis, is assumed to occur in the plane defined by the tangent vector to the epidermal surface $\mathbf{n}_x$ and $\mathbf{n}_y$ as described in Fig. 2.

The mechanical properties of the skin have been reported as both isotropic[27,26] and anisotropic[36,19]. The isotropy and the different levels of anisotropy have been reported for different parts of the skin and species, presenting mechanical differences. Here, and given the lack of data on the structure of the skin in the finger tip we opted for a simple isotropic model, defined by a isotropic strain energy function. We chose a Neo-Hookean

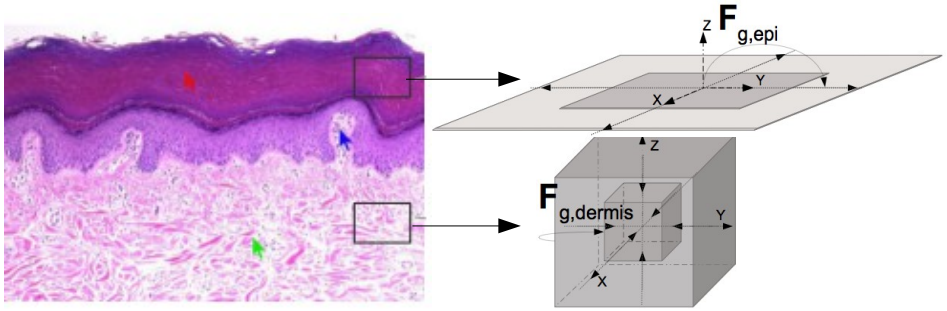

Figure 2: On the right, histology of the skin modified from[6]. Red arrow indicates the outer layer of the dermis, the stratum corneum. Blue and green arrows indicate the papillary and reticular dermis. After immersion in water, the epidermis swells and the hypodermis contracts. The swelling and contraction mechanism is described by the deformation gradient $\mathbf{F}_{\mathrm{g,\,epi}}$ and $\mathbf{F}_{\mathrm{g,\,dermis}}$ respectively, as shown in the top and bottom right hand side of the picture.

model as

$$\Psi_{\mathrm{elas}}(\overline{I}_1) = \mu[\overline{I}_1 - 3] \tag{11}$$

where μ is a stress-like parameter and $\overline{I}_1$ is the first invariant of the isochoric part of the deformation. Material parameters are obtained from[27,26]. These values were reported as $\mu_{epi} = 0.16$ MPa and $\mu_{dermis} = 9.4$ kPa for the epidermis and the dermis respectively. The hypodermis has a Young's Modulus of 0.12kPa.

2.3 Finite element model and numerical implementation

A 3D model of a human index finger is reconstructed from geometrical features of a STereoLithography[57] file of a finger reconstructed under Commons Attribution-Non

Commercial-Share Alike license. The finite element mesh consists of 624996 linear hexahedral elements with hybrid formulation with a total of 1964760 degrees of freedom which allowed us to follow the folding pattern with high accuracy. The epidermis layer was modeled bottom-up using layers with a total thickness of 0.25 mm. The dermis was modeled with an idealized constant thickness of 1.2 mm. The connective tissue between the dermis and the bone, the hypodermis, is composed of loose fatty connective tissue. A sketch of the geometry is presented in Fig. 3.

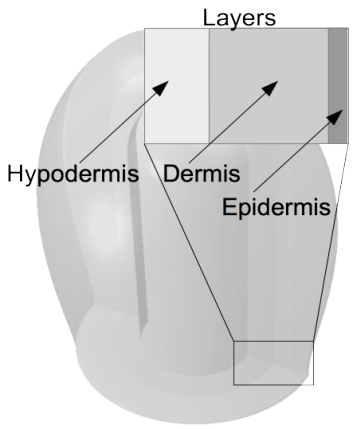

Figure 3: Sketch of the finger tip geometry. The different skin layers are highlighted. The idealized bone structure is presented at the back of the translucent tissue.

We solve the boundary value problem as a pseudo-static problem in the non-linear general purpose finite element program ABAQUS. For every pseudo-static step in the non-linear incremental procedure, the pseudo-time $t \in [0, 1]$ is defined as the interval of pseudo-times in which the non-linear solution is solved incrementally.

We introduce the swelling/contraction mechanism through the growth multiplier ϑ in

a UMAT subroutine from where the energy, stress and constitutive moduli are defined. We use a linear evolution of the growth multiplier with the pseudo-time as $\vartheta_{epi} = 1+\vartheta_{epi}^{max}t$ and $\vartheta_{dermis} = 1 - (\vartheta_{dermis}^{min} - 1)t$. The multiplier is defined as an internal variable stored in the integration point of the finite element model. We successively calculate the growth multiplier ϑ, the growth tensor $\mathbf{F}_g$, the elastic tensor $\mathbf{F}_e$ as well as the Piola-Kirchoff stress tensor $\mathbf{S}$ and the tangent moduli $\mathbf{C}$, essential for an implicit implementation in a finite element framework (see Section 2.1).

Due to the non-linear instabilities of the wrinkling problem we monitor the convergence of the problem. We used an adaptive time stepping since a fixed time stepping scheme either failed or resulted in extremely long simulation times due to the small time steps required. The time increment is decreased or increased automatically depending on the convergence of the Newton-Raphson iteration. Our model has proven to be inherently stable using time adaptive stepping and we did not need to adopt further measures as Riks or Arc Length methods for buckling and instabilities analysis[54,48].

We imposed three boundary conditions in the model (see Fig. 3) for reference). The first one is in the cutting plane of the finger, corresponding to a transversal cut at the first phalanx, with zero displacement in the normal direction to the cutting plane. Secondly, to mimic the effect of the phalanx, the bone where the tissue is attached to, we included a cylindrical geometry in the middle of the finger representing the attachment of the tissue with the bone. Therefore, zero displacements were imposed in this part of the model. Note that the real geometry of the bone differs from a idealized cylinder mainly in the

section close to the bone joints. However, in the section of the finger tip bulb the bone follows more closely a cylinder-like shape. And thirdly, we also imposed zero displacement in the normal direction to the longitudinal cutting plane. This cut lies on a plane below the point of nail insertion to the finger, where the displacement of the tissue is allowed in the normal direction of the skin surface. It is worth mentioning that the nail, which can restrict tissue displacement, is in the uppermost plane of the finger in relation with the palm, above the cutting plane of the model and, therefore, the effect of the nail is not considered without loss of generality. It is worth to note that we do not have experimental evidence to quantitatively define the values of the boundary conditions but, qualitatively and given the lack of experimental data, we believe they are a good assumption.

3 Results

We present comparative results for different contraction and swelling levels, individually and coupled, of the wrinkling process. In order to assess the appearance of the wrinkles, we follow a simple assumption. We measure the ratio of the maximum and minimum value of the maximum principal strains. This ratio gives us an idea of the wrinkling formation since the maximum values is associated with the valley of the wrinkle and the minimum is associated with the tip of the wrinkle. Lacking a more precise definition of this threshold, we choose a value of 1.075. This value was chosen as the value by which the wrinkles were observed to the naked eye. Although other indicators could be used, the choice of this particular one is suitable for comparatives purposes.

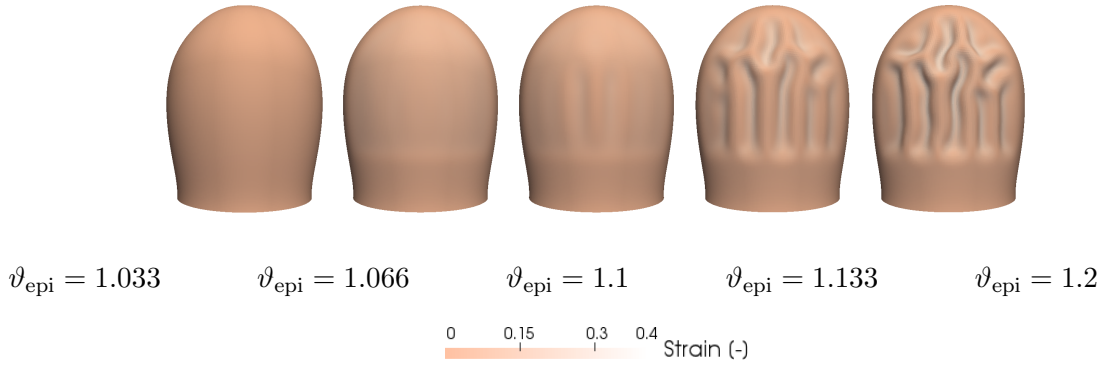

Figure 4: Results of simulated wrinkles with epidermal swelling only. Subfigures show the wrinkled states for $\vartheta_{\text{epi}} = 1.03, 1.066, 1.10, 1.13, 1.20$. The color code shows the level of maximum principal strain induced in the skin due to the wrinkling process.

3.1 Individual effect of the 'shrink' and 'swell' models

First, we performed an exploration of the swelling parameter ϑ_{epi} without contraction of the dermis. This case is motivated by experimental observation. It is known that patients with neural system disorders do not experience wrinkles and it is believed that this is due to the impairment of the contraction of the vasculature in the lower layer of the skin. We show the evolution of the wrinkles for different values of $\vartheta_{\text{epi}} \in [1, 1.2]$ in Fig. 4. It shows that the wrinkles start to appear at $\vartheta \approx 1.1$, which is an increase of area in $\approx 10\%$.

Secondly, we perform a parametric study of the contraction parameter $\vartheta_{\text{dermis}}$. This case represent a situation where the contraction of the vasculature is allowed but the osmosis of the epidermis is not. In Fig. 5 we show the evolution of the wrinkling process for different values of $\vartheta_{\text{dermis}} \in [0.5, 1]$. In this case, the folds start to appear at $\vartheta \approx 0.83$.

To achieve wribkles comparable to $\vartheta_{\text{epi}} = 1.2$, the contraction level had to be decreased

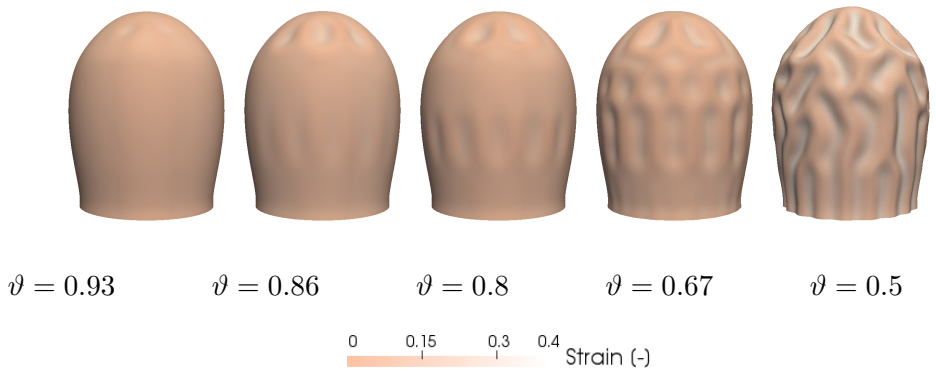

Figure 5: Results of simulated wrinkles with dermal contraction only. Subfigures show the wrinkled states for $\vartheta_{\text{dermis}} = 0.93, 0.86, 0.8, 0.67, 0.5$. The color code shows the level of maximum principal strain induced in the skin due to the wrinkling process.

up to $\vartheta_{\text{dermis}} = 0.5$, as observed in Fig. 4 and 5. For the same level of swelling and contraction, the swelling phenomenon seems to have a larger effect on the formation of wrinkles. These results indicate that the layer in the outer convex layer dominates the evolution of the wrinkles.

3.2 Coupled effect of the 'shrink' and 'swell' models

Thereafter, we investigated both mechanisms acting together. The problem with $\vartheta_{\text{epi}}^{max} = 1.1$ and $\vartheta_{\text{dermis}}^{max} = 0.5$, presented in Fig. 6, is analyzed. This choice was motivated by the above results on the swelling of the epidermis. We wanted to analyze the combination of different contraction levels in the range of swelling where no wrinkles are observed under no contraction. As it was argued before, this range of swelling is proposed as the physiological range of epidermic swelling due to osmosis.

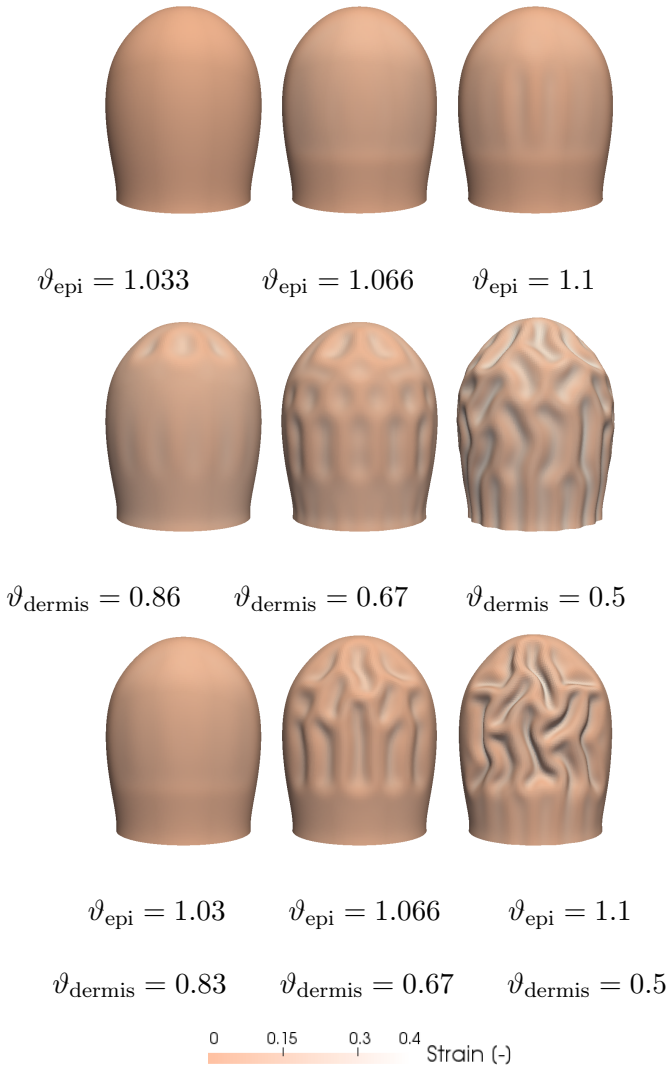

Figure 6: Results of simulated wrinkles when a simultaneous swelling of the epidermis and contraction of the dermis occurs with $(\vartheta_{\text{epi}}, \vartheta_{\text{dermis}}) = (1.03, 0.83), (1.066, 0.67)$ and $(1.1, 0.5)$. Subfigures in the first and second row show the wrinkled state for the swelling and contraction problem alone for comparative purpouses. The third row shows the effect of both mechanism combined. The color code shows the level of strain induced in the skin due to the wrinkling process.

Results in Fig. 6 reported first evidences of the coupling effect. For $\vartheta_{\text{epi}} = 1.033$ and $\vartheta_{\text{dermis}} = 0.86$, which represents a larger value of contraction than swelling, no wrinkles were formed. No wrinkles were neither formed for the individual mechanism acting separately. For $\vartheta_{\text{epi}} = 1.066$, $\vartheta_{\text{dermis}} = 0.67$ the wrinkles clearly appeared even though when they were simulated separately they were almost imperceptible. In the last simulation, $\vartheta_{\text{epi}} = 1.1$ and $\vartheta_{\text{dermis}} = 0.5$, the resulting wrinkles for the coupled mechanisms were very significant. Note that, in this case, the level of contraction was very large and, probably, out of the physiological range. From these results we can see that the amount of shrinking needed for the formation of wrinkles is much larger that the amount of swelling in the epidermis and that when both mechanism are coupled the wrinkling process evolves faster than individually.

Next, to broaden the parametric study, a symmetric range of swelling/contraction levels is performed for the sake of completeness of the results. We imposed $\vartheta_{\text{epi}}^{max} = 1.2$ and $\vartheta_{\text{dermis}}^{max} = 0.8$ (Fig. 7).

For small changes in the contraction and swelling ($\vartheta_{\text{epi}} = 1.066$, $\vartheta_{\text{dermis}} = 0.93$) the wrinkling pattern starts to appear, even though the individual mechanisms did not show any wrinkles at this level (Fig. 7, bottom row). For $\vartheta_{\text{epi}} = 1.133$ and $\vartheta_{\text{dermis}} = 0.86$ large folds appear when, at the same level the wrinkling was for the individual effects was imperceptible. These results confirms that the increasing values of the swelling is the determining mechanism in the wrinkling process. In this latter case, the level of contraction is much higher than in the second column of Fig. 7 (0.86&0.67) however

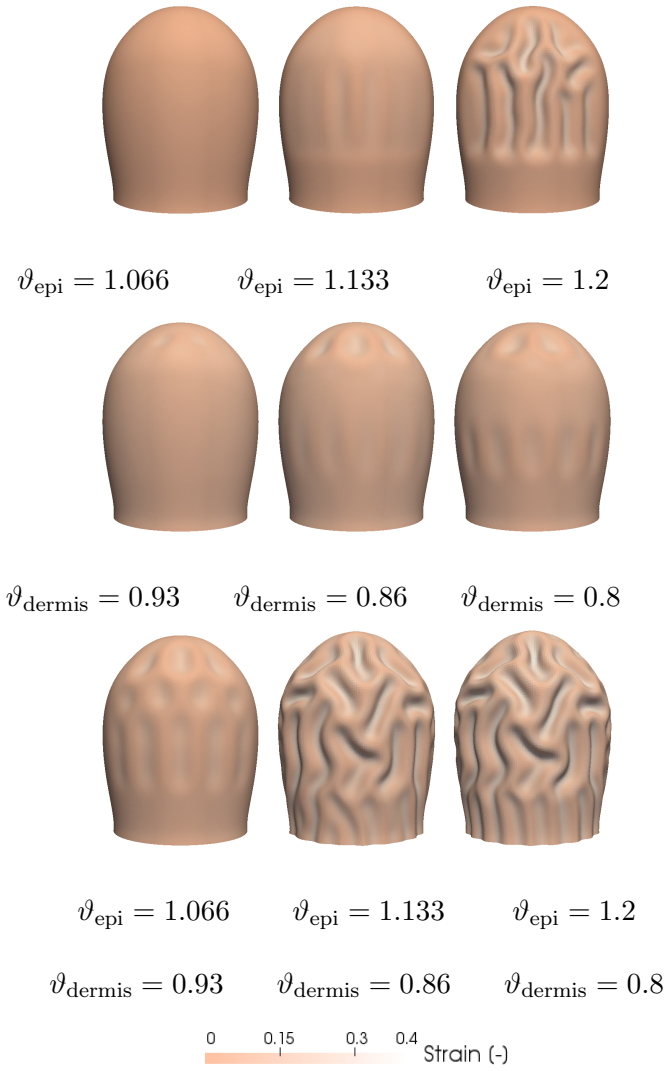

Figure 7: Results of simulated wrinkles when a simultaneous swelling of the epidermis and contraction of the dermis occurs with $(\vartheta_{\text{epi}}, \vartheta_{\text{dermis}}) = (1.066, 0.93), (1.133, 0.86),$ and $(1.2, 0.8)$. Subfigures in the first and second row show the wrinkled state for the swelling and contraction problem alone for comparative purpouses. Third row shows the effect of both mechanism together. The color code shows the level of strain induced in the skin due to the wrinkling process.

larger wrinkles appear here, showing that the contraction of the dermis less effective than swelling of the epidermis. At $\vartheta_{\text{epi}} = 1.2$ and $\vartheta_{\text{dermis}} = 0.8$ a similar folding pattern to the previous case can be observed. It is worth noting that the folding pattern observed in the last two cases of Fig. 7 seems larger than what it is usually observable in-vivo. This is an expected result since it exceeds the previously established threshold for a physiological swelling and contraction levels.

4 Discussion

Everyone has experienced wrinkly fingers after an extended exposure to water. These wrinkles have been proposed as an evolutionary mechanism for a better grip of wet objects[23,40]. However, besides experimental observations[7,55,33] or mathematical theories[31,53,58,16] there is still not a clear agreement whether this is a result of the contraction of the hypodermis (the 'shrink' model), the effect of epidermal swelling (the 'swell' model), or the coupling of both mechanisms. Yin and co-wokers performed a similar computational approach as the one adopted in the present work[53], however, did not include the contraction of the deeper layers of the skin which has been proved to play a fundamental role in the formation of wrinkles[7,55] .

The mechanism of differential swelling in conforming substrates has been a classical problem in mechanics[30,31,58].The main focus of attention has been on the differential stiffness of the substrate and the relative thickness which lead to distinctive folding patterns[31,58] and buckling phenomena[3,25] in different kind of materials[2,39,15,9]. In this con-

tribution we focused on the formation of finger wrinkles without considering the effect of differential stiffness and thickness, therefore, on the simple goal of determining the appearance or not of wrinkles based on mechanical and geometrical experimental data. For a further details on the stiffness and relative thickness on pattern formation we refer to the above mentioned references.Skin has also a documented pre-stretch state in vivo. In several locations the level of pre-stretch has been documented in the range of . However, and to the best of our knowledge no information of such mechanism has been reported in the finger tip. In order to not induce further uncertainties in our model we opted for not including such phenomenon in out model. Other models have been reported in literature to deal with the pre-stretch state in the skin[52,11,22].

To investigate this problem, computational mechanics was used to test this phenomenon *in-silico* by imposing not only the swelling of the epidermis but also the shrinking of the hypodermis. Three different kind of simulations were performed: (1.) the individual effect of the contraction, (2.) the individual effect of the swelling in external layers of the skin and (3.) the coupling of both phenomena together.

First, we investigated the swelling of the epidermis alone. Experimental observations of patients with non wrinkly fingers, which is assumed to be due to impairment of nervous function[7,55], suggest that the maximum swelling that the epidermis can reach is not high enough to induce wrinkles, otherwise, this folding pattern would be observable in patients with neurological disorders. Our results on the epidermis swelling alone shown that the swelling levels that do not induce wrinkling are below $\approx 10\%$. Wrinkles appear above this

threshold contradicting experimental results in patients with neural system disorders, who are incapable of generating contraction. Therefore, we conclude that the amount of swelling should be lower than $\approx 10\%$.

The effects of the contraction of the dermis alone were also investigated. We observed that a larger contraction level has to be reached, compared with the swelling of the epidermis, to achieve similar wrinkles. To obtain a similar wrinkling pattern the dermis had to be contracted up to a 50% of its initial volume. This high contraction seems to be out of physiological bounds, since it would imply that the vasculature is made of 50% of the tissue volume and that it would be entirely collapsed inward.

Finally, the coupling effect of epidermal swelling and dermis contraction was analyzed. First, the threshold value for the swelling established above (up to $\vartheta_{\text{epi}} = 1.1$) and a contraction of $\vartheta_{\text{dermis}} = 0.5$ was used. When the epidermis is expanded in the range of $\approx 5 - 10\%$, a small level of contraction produce a significant wrinkling in the fingertip. Note that any of these levels of swelling and contraction were not enough by themselves to produce wrinkles. In conclusion, both mechanisms have to work together in order to observe wrinkles in the fingertips. Therefore, a combination of both hypotheses, the 'shrink' and the 'swell' approaches, are required to create significant wrinkling within the physiological swelling and contraction limits.

In this work, by means of computational models from continuum mechanics, we were able to determine what mechanism is responsible for wrinkly fingers. We conclude that both the contraction and the swelling of the different layers of the skin are required to

induce wrinkles in the fingertips. We have demonstrated that computational models are able to define threshold levels for the trigger of the wrinkling process based on the swelling and contraction mechanism which are not objectively defined in the medical protocols. This is an key result since it could be used for the diagnosis of patients affected by neurological disorders. The fact that the swelling of the epidermis has a larger effect on the wrinkling of the fingertip than the contraction of the vasculature can have an impact on medical diagnosis. We observed that relatively small variations in the swelling level have a higher impact than the contraction of the dermis. Therefore, the outcome of medical exams could be biased by the level of epidermis expansion achieved in a specific patient. Both the contraction and expansion mechanisms have been considered here to evolve linearly and independently from each other. Although this is a simple assumption, we are not aware of any experimental data that show an eventual influence of each other or of a non-linear evolution. In this study we have used only one slightly idealized geometry with constant layer thickness but the low variability on these factors support this approach. Some of the previous references in differential swelling has study the effect of different curvature in the layers on the final wrinkling pattern. Although the different geometry or curvature among the different fingers could induce some differences in folding pattern, we believe that they should not change dramatically given the relatively uniform geometry of the human fingers. Without doubt, further experiments will help to close the debate about the origin of fingertip wrinkling. In that direction, experiments canceling out the osmosis in the epidermis, in order to isolate and study dermal contraction, have not been

performed yet. It should be possible to achieve them using an impermeable barrier on the epidermis surface. We propose this future work for the experimental biologist interested in the problem of wrinkly fingers.

References

[1] Ambrosi, D. and Ateshian, G.A. A and Arruda, E.M. M and Cowin, S.C. C and Dumais, J. and Goriely, A. and Holzapfel, G.A. A and Humphrey, J.D. D and Kemkemer, R. and Kuhl, E. and Olberding, J.E. E and Taber, L.A. A and Garikipati, K. Perspectives on biological growth and remodeling. J. Mech. Phys. Solids, 59:863–883, 2011.

[2] Balbi, V. and Kuhl, E. and Ciarletta, P. Morphoelastic control of gastro-intestinal organogenesis: Theoretical predictions and numerical insights, J. Mech. Phys. Solids,78, 2014.

[3] Ben Amar M, Goriely, A. Growth and instability in elastic tissues. J. Mech. Phys. Solids, 53(10):2284–2319, 2005.

[4] Ben Amar M, Ciarletta P. Swelling instability of surface-attached gels as a model of soft tissue growth under geometric constraints. J Mech Phys Solids. 58(7):935–954, 2010.

[5] Ben Amar M, Jia F. Anisotropic growth shapes intestinal tissues during embryogenesis. Proc Natl Acad Sci U S A. 110(26):10525–30, 2013.

[6] Blugerman G., Paul M. D., Schavelzon D., Mulholland R. S., Sandhoffer M., Lisborg P., Rusciani A., Divaris M. and Kreindel M. Radio-Frequency Assisted Liposuction (RFAL), Advanced Techniques in Liposuction and Fat Transfer. Prof. NIkolay Serdev (Ed.), ISBN: 978-953-307-668-3, InTech.

[7] Braham J., Sadeh M., Sarovapinhas I.. Skin wrinkling on immersion of hands: a test of sympathetic function Arch. Neurol., 36(2):113–114, 1979.

[8] Budday S., Raybaud C., and Kuhl E.. A mechanical model predicts morphological abnormalities in the developing human brain. Sci. Rep., 4:5644, 2014.

[9] Budday S., Steinmann P., and Kuhl E. The role of mechanics during brain development. J. Mech. Phys. Solids, 72:75–92, 2014.

[10] Changizi M., Weber R., Kotecha R., Palazzo J. Are Wet-Induced Wrinkled Fingers Primate Rain Treads? Brain Behav Evol 77:286–290, 2011.

[11] Chaudhry HR, Bukiet B, Findley T, Ritter AB Evaluation of Residual Stress in Rabbit Skin and the Relevant Material Constants J Theor Biol, 2:191–195, 1998

[12] Ciarletta P, Ben Amar M, Labouesse M. Continuum model of epithelial morphogenesis during Caenorhabditis elegans embryonic elongation. Philos Trans A Math Phys Eng Sci. 367(1902):3379–400, 2009.

[13] Ciarletta P, Ben Amar M. Pattern formation in fiber-reinforced tubular tissues:

Folding and segmentation during epithelial growth. J Mech Phys Solids. 60(3):525–537, 2012.

[14] Ciarletta P, Ben Amar M. Peristaltic patterns for swelling and shrinking of soft cylindrical gels. Soft Matter. 8(6):1760, 2012.

[15] Ciarletta, P. and Balbi, V. and Kuhl, E. Pattern selection in growing tubular tissues, Phys. Rev. Lett., 113, 2014.

[16] Cao Y. and Hutchinson J. W. From wrinkles to creases in elastomers: the instability and imperfection-sensitivity of wrinkling. P Roy Soc A-Math Phy, 468(2137):94–115, 2012.

[17] Efimenko K, Rackaitis M, Manias E, Vaziri A, Mahadevan L, Genzer J. Nested self-similar wrinkling patterns in skins. Nat Mater. 4(4):293–7, 2005.

[18] Eskandari M., Kuschner W.G., and Kuhl E.. Patient-Specific Airway Wall Remodeling in Chronic Lung Disease. Ann. Biomed. Eng., pages 1–14, 2015.

[19] Bryan F. Dynamic mechanical testing of human skin 'in vivo' J. Biomech.,6(3), 1970

[20] Flory PJ. Thermodynamic relations for high elastic materials. T Faraday Soc, 57: 829–838, 1961.

[21] Flynn CO, McCormack BAO. A three-layer model of skin and its application in simulating wrinkling. Comput Methods Biomech Biomed Engin. 2009 feb;Available from:

[22] Flynn C, McCormack BAO. Simulating the wrinkling and aging of skin with a multi-layer finite element model. J Biomech. 43(3):442–8, 2010.

[23] Frenzel H, Bohlender J, Pinsker K, Wohlleben B, Tank J, Lechner SG, Schiska D, Jaijo T, Rueschendorf F, Saar K, Jordan J, Millan JM, Gross M , and Lewin GR. A Genetic Basis for Mechanosensory Traits in Humans. PLOS Biol., 10(5), May 2012.

[24] Goektepe S, Abilez OJ, and Kuhl E. A generic approach towards finite growth with examples of athlete's heart, cardiac dilation, and cardiac wall thickening. J. Mech. Phys. Solids, 58(10), 1661–1680, 2010.

[25] Goriely A, Ben Amar M. Differential growth and instability in elastic shells. Phys Rev Lett. 94(19):198103, 2005.

[26] Hendriks FM, Brokken E, Oomens CWJ , Bader DL, Baaijens FPT A numerical-experimental method to characterize the non-linear mechanical behaviour of human skin. Med Eng Physics 28(3), 259–266

[27] Hendriks FM, Brokken D, Van Eemeren JTWM, Oomens CWJ, Baaijens FPT, Horsten JBAM The relative contributions of different skin layers to the mechanical behavior of human skin in vivo using suction experiments. Skin Res Technol. 9(3), 1600–0846

[28] Himpel G, Kuhl E, Menzel A, and Steinmann P. Computational modelling of isotropic multiplicative growth. CMES- Comp Model Eng, 8(2), 119–134, 2005.

[29] Holzapfel G. Nonlinear Solid Mechanics: A Continuum Approach for Engineering. John Wiley & amp; Sons

[30] Huang Z, Hong W, Suo Z. Evolution of wrinkles in hard films on soft substrates. Phys Rev E Stat Nonlin Soft Matter Phys. 70(3):030601,2004.

[31] Huang ZY, Hong W, Suo Z. Nonlinear analyzes of wrinkles in a film bonded to a compliant substrate. J Mech Phys Solids. 53(9):2101–2118, 2005.

[32] Jones GW, Chapman SJ Modeling Growth in Biological Materials. Siam review. 54(1), 52–118, 2012.

[33] Kareklas K, Nettle D, and Smulders TV. Water-induced finger wrinkles improve handling of wet objects. Biol Lett, 9(2): 20120999, 2013.

[34] Kuhl E, Steinmann P. Theory and numerics of geometrically non-linear open system mechanics. Int J Numer Meth Eng. 58(11):1593–1615, 2003.

[35] Kuhl E. Growing matter: a review of growth in living systems. J Mech Behav Biomed Mater. 29:529–43, 2014.

[36] Lanir Y, Fung YC. J Biomech, 2(7): 171–174, 1974 Two-dimensional mechanical properties of rabbit skin–II. Experimental results

[37] Lambert, WC Physiology, Biochemistry, and Molecular Biology of the Skin New Eng J Med, 328(14):1048–1048, 1993.

[38] Lee EH. Elastic-plastic deformation at finite strains. J Appl Mech, 36(1):1–&, 1969.

[39] Li B, Cao YP, Feng XQ, Gao H. Surface wrinkling of mucosa induced by volumetric growth: Theory, simulation and experiment. J Mech Phys Solids. 59(4):758–774, 2011

[40] Lin HT, Hong TF, and Li WL. Grip Performance Affected by Water-Induced Wrinkling of Fingers. Tribol. Lett., 58(3):1–9, 2015.

[41] Liu Y, Yang X, Cao Y, Wang Z, Chen B, Zhang J, Zhang H. Dehydration of core/shell fruits Comp Graphics 47, 68 – 77, 2015.

[42] Marsden JE, Hughes TJR. Mathematical Foundations of Elasticity. Dover Publications .

[43] Menzel A, Kuhl E. Frontiers in growth and remodeling. Mech Res Commun. 42:1–14, 2012.

[44] Mora T, Boudaoud A. Buckling of swelling gels. Eur Phys J E Soft Matter. 20(2):119–24, 2006.

[45] Motala MJ, Perlitz D, Daly CM, Yuan P, Nuzzo RG, Ralph G and Hsia JK Programming matter through strain. Ext. Mech. Lett., 3:8–16, 2015.

[46] Moulton DE, Goriely A. Circumferential buckling instability of a growing cylindrical tube. J Mech Phys Solids. 59(3):525–537, 2011.

[47] O'Riain S. New and simple test of nerve function in hand. Br Med J, 3(5881):615–6, 1973.

[48] Riks E. An incremental approach to the solution of snapping and buckling problems. Int J Solids Struct, 15(7):529 – 551, 1979.

[49] Rodriguez EK, Hoger A, and McCulloch AD. Stress-dependent finite growth in soft elastic tissues. J Biomech, 27(4):455–467, 1994.

[50] Saez P On the theories and numerics of continuum models for adaptation processes in biological tissues. Arch Comput Method E DOI: 10.1007/s11831-014-9142-8

[51] Stoop N, Lagrange R, Terwagne D, Reis PM, Dunkel J. Curvature-induced symmetry breaking determines elastic surface patterns. Nat Mater. 14(3):337–42, 2015.

[52] Tong P, Fung YC The stress-strain relationship for the skin J Biomech, 9(10):649–657, 1976

[53] Yin J, Gerling GJ, and Chen X. Mechanical modeling of a wrinkled fingertip immersed in water. Acta Biomater., 6(4):1487–1496, 2010.

[54] Wempner GA. Discrete approximations related to nonlinear theories of solids Int J Solids Struct, 11:1581 – 1599, 1971

[55] Wilder-Smith EPV. Water immersion wrinkling–physiology and use as an indicator of sympathetic function. Clin Auton Res, 14(2):125–131, 2004.

[56] Wilder-Smith EPV and Chow A. Water-immersion wrinkling is due to vasoconstriction. Muscle Nerve, 27(3):307–11, 2003.

[57] http://www.muffler.123dapp.com/123C-3D-Model/Finger-Index/866442

[58] Zang J, Zhao X, Cao Y, and Hutchinson JW. Localized ridge wrinkling of stiff films on compliant substrates. J. Mech. Phys. Solids, 60(7):1265 – 1279, 2012.

[59] Zhao Y, Han X, Li G, Lu C, Cao Y, Feng XQ, et al. Effect of lateral dimension on the surface wrinkling of a thin film on compliant substrate induced by differential growth/swelling. J Mech Phys Solids. 83:129–145, 2015.